atmosphere

MDPI

Article

The Roles of Atmospheric and Air–Sea Interaction Processes in Causing the Eastward Extension of the Western North Pacific Monsoon Trough in Boreal Summer

Chi Qin [1] and Tim Li [1,2,*]

[1] Key Laboratory of Meteorological Disaster, Ministry of Education (KLME)/Joint International Research Laboratory of Climate and Environmental Change (ILCEC)/Collaborative Innovation Center on Forecast and Evaluation of Meteorological Disasters (CIC-FEMD), Nanjing University of Information Science and Technology, Nanjing 210044, China; 20191101027@nuist.edu.cn

[2] Department of Atmospheric Sciences, School of Ocean and Earth Science and Technology, University of Hawaii at Manoa, Honolulu, HI 96822, USA

* Correspondence: timli@hawaii.edu

Abstract: What causes the eastward extension of the climatological monsoon trough over the western North Pacific in the boreal summer was investigated through both observational analyses and numerical simulations. It was found that the highest SST is always located to the east of maximum precipitation, and this asymmetric SST pattern favors the eastward extension of the monsoon trough through SST induced boundary layer convergence. A mixed-layer heat budget analysis further indicates that the SST asymmetry arises primarily from the asymmetric pattern of cloud-modified downward shortwave radiation. In addition, two internal atmospheric mechanisms are identified. Firstly, there is a zonal asymmetry in the lower-tropospheric moisture advection. Southeasterlies to the east of the convection, in association with the subtropical high advect high mean moisture from south, leads to low-level moistening to the east of the convective center. Secondly, the heating-induced Kelvin wave response leads to a boundary layer convergence ahead of the convection. Both the processes lead to the setup of a convectively unstable stratification to the east, favoring the eastward extension of the monsoon trough. Two sets of the WRF model experiments that specify a fixed and a time-dependent SST field confirm the roles of the aforementioned atmospheric internal processes as well as the air–sea interaction process in causing the eastward progression of the climatological monsoon trough over the western North Pacific.

Keywords: monsoon trough; climatological pentad mean; moisture advection

Citation: Qin, C.; Li, T. The Roles of Atmospheric and Air–Sea Interaction Processes in Causing the Eastward Extension of the Western North Pacific Monsoon Trough in Boreal Summer. *Atmosphere* **2023**, *14*, 750. https://doi.org/10.3390/atmos14040750

Received: 14 March 2023
Revised: 10 April 2023
Accepted: 18 April 2023
Published: 21 April 2023

1. Introduction

A unique feature in the tropical western North Pacific (WNP) is the occurrence of a monsoon trough (MT), where the low-level monsoon westerlies meet trade easterlies [1]. MT is characterized by low sea level pressure, intense precipitation, pronounced low-level convergence, and mid-tropospheric ascending motions [2]. MT provides favorable dynamic and thermodynamic environments for tropical cyclone (TC) formations [3,4], and its variation has a great impact on TC genesis locations, times, and frequencies, as well as the TC track [5–7].

The formation of the WNP MT is conventionally thought to be driven by the meridional gradient of the hemispherically asymmetric sea surface temperature [1,8]. The asymmetric solar radiation forcing in the boreal summer induces a northward cross-equatorial flow in the lower troposphere, which converges onto the summer hemisphere, leading to enhanced precipitation north of the equator. This is a major mechanism for the formation of an oceanic monsoon, as discussed by Wang et al. [8]. Different from this traditional thermodynamic mechanism, Qin et al. [9] proposed a pure atmospheric dynamics mechanism. They

constructed a nonlinear barotropic vorticity model with a specified background flow, following Kuo et al. [10]. As synoptic-scale easterly waves specified over the eastern boundary of the model propagated westward [11], they tended to contract under the background flow. Due to the vorticity segregation process, eddies with positive vorticities shifted to the north, while eddies with negative vorticities shifted to the south. This led to the formation of a pair of large-scale cyclonic and anticyclonic circulations, straddling the central reference latitude. The so-generated large-scale circulation could be further enhanced through moisture–circulation–convection feedback.

An interesting feature of the time evolution of the climatological MT is the eastward extension of precipitation and low-level westerly. In June, the monsoon westerly is confined to the west of the Philippines. Then, it gradually expands eastward into the western Pacific. In late July, the monsoon westerly extends to 150° E. It continues expanding eastward in August, and it starts to dissipate after that [12]. Therefore, the eastward extension of the monsoon westerly and precipitation from June to August signifies the development of the MT over the WNP.

An interesting question is what causes the eastward extension of the climatological monsoon trough. Wu [13] suggested that it might be attributed to local air–sea interaction. Wu [13] found that the change in SST associated with the surface heat flux anomaly might play a role in promoting the eastward extension of the MT. However, as shown by our idealized model simulation, MT can still extend eastward even with a specified time-independent SST in the boreal summer. This implies that atmospheric internal processes may also play a role.

Motivated by the rationale above, we intend to reveal specific atmospheric and air–sea interaction processes that are responsible for the climatologically subseasonal evolution of the MT, taking both observational analysis and numerical modeling approaches. The remaining part of this paper is organized as follows. In Section 2, we describe the data and model experiment design. The observational analyses of atmospheric and oceanic fields associated with the eastward extension of the MT are described in Section 3. In Section 4, we discuss the idealized WRF experiment results. Finally, a conclusion and discussions are given in the last section.

2. Data, Model Experiment Design, and Analysis Method

2.1. Data

The European Centre for Medium-Range Weather Forecasts interim reanalysis (ERA-Interim) datasets with a resolution of 1° × 1° at 6 h intervals [14] were employed in this study for both observational analyses and numerical model simulations (as initial and lateral boundary conditions). In addition, the precipitation field from the Tropical Rainfall Measuring Mission (TRMM) 3B42 version 7 dataset was used. This dataset had a 3 hourly temporal resolution and a horizontal resolution of 0.25° [15].

In addition, three-dimensional ocean temperature fields used in this study were obtained from the National Center for Environmental Prediction (NCEP) Global Ocean Data Assimilation system (GODAS) products. The GODAS product had a resolution of 1° in zonal and 1/3° in the meridional direction and 40 vertical levels with a 10 m resolution in the upper 200 m. The surface heat flux field used for this study was taken from various datasets. The latent and sensible heat flux data were obtained from the Objectively Analyzed Air–Sea Fluxes for the Global Oceans (OAFlux) product, with a 1° × 1° resolution. The surface radiation flux fields were extracted from the Japanese 55-year Reanalysis Project (JRA-55), with a 1.25° × 1.25° resolution.

The analysis period for all the data spanned from 1998 to 2017, with a focus on boreal summer months from June to August. To reveal the detailed evolutions of climatological atmospheric and oceanic fields, pentad (5-day) mean fields were constructed for each year. For all the variables (precipitation, u, v, SST, flux terms, and so on), pentad means were constructed for each year since June 1st. Additionally, climatological pentad means were calculated as multi-year means.

2.2. Model Experiment Design

The Advanced Research Weather Research and Forecasting system (WRF-ARW, Version 3.8) was utilized in this study. The model had a horizontal resolution of 50 km and a vertical resolution of 46 vertical layers, with a model top at 10 hPa. The mesh sizes were 200 × 130, and the model domain was large enough to cover most of the WNP. The simulations utilized various physical parameterization schemes, including the Yonsei University (YSU) planetary boundary layer (PBL) scheme, the WRF single moment 6-class scheme, and the RRTM longwave radiation and Dudhia shortwave radiation schemes.

Two sets of numerical experiments were carried out. In the control experiment (CTL), variables from the ERA-Interim datasets, including surface pressure, wind fields, geopotential height, temperature, SST, and specific humidity, were used as the initial and lateral boundary conditions [16]. The objective of this control experiment is to simulate a realistic eastward extension of the WNP monsoon trough in the presence of realistic SST evolution from June 1 to August 31. In the sensitivity experiment (FIX_SST), SST was kept to the climatological pattern on June 1, while other settings were same as in the control experiment. The model simulated 3-dimensional meteorological fields, including wind, temperature, geopotential height, and specific humidity fields. The reanalysis product was used as the model's initial condition without spin-up or the use of an initialization scheme, as a data assimilation method had been applied when the reanalysis product was generated.

The purpose of the sensitivity experiment was to reveal whether or not the MT would extend eastward with a fixed SST. By comparing the two experiments, one may reveal the relative role of the atmospheric and oceanic processes in promoting the eastward extension of the MT. For each of the experiments above, the model was integrated for 92 days. There was a sponge layer (about 20 grids) in the lateral boundary layers so that observed lateral boundary conditions could be well represented. Same as the observational data, the pentad mean data of the simulation results were constructed prior to the data analysis.

2.3. Analysis Method

To understand the cause of SST asymmetry relative to the monsoon convection, the ocean mixed layer heat budget was diagnosed following Li et al. [17]. The time change rate of the mixed-layer averaged temperature may be written as follows:

$$\frac{\partial T}{\partial t} = -u\frac{\partial T}{\partial x} - v\frac{\partial T}{\partial y} - w\frac{\partial T}{\partial z} + \frac{Q_{net}}{\rho c_w H} + R, \quad (1)$$

$$Q_{net} = Q_{SW} + Q_{SW} + Q_{LH} + Q_{SW}, \quad (2)$$

where T denotes the mixed layer temperature, and u, v, and w are three-dimensional ocean current velocities. Q_{net} denotes the net surface heat flux term that includes surface shortwave (Q_{SW}) and longwave radiation (Q_{LW}) and latent (Q_{LH}) and sensible (Q_{SH}) heat fluxes (with all positive values denoting downward, i.e., the ocean receives heat), R denotes the residual term, ρ is the density of water (= 10^3 kg m^{-3}), C_w is the specific heat of water (= 4000 Jkg^{-1}K^{-1}), and H denotes the mixed layer depth. The mixed layer depth is defined as a depth where ocean temperature is 0.5 °C below the surface temperature.

3. Processes Associated with Eastward Extension of WNP MT

In this section, we intend to reveal specific atmospheric and air–sea interaction processes responsible for the eastward MT extension, based on observational analyses. Figure 1 illustrates how the climatological monsoon trough marches eastward during June–August. It depicts the time–longitude sections of the climatological pentad mean precipitation, SST, and 850 hPa zonal wind averaged over the key MT latitudinal zone (10° N–15° N) during the entire summer months (Pentad 1–18, from June 1 to August 31). Note that the monsoon westerly at this zone is confined to the west of the Philippines in early June, and it then gradually penetrates into the western Pacific (east of the Philippines). It fi-

nally reaches about 150° E in Pentad 18. Accompanied by the low-level westerly are the eastward expansion/migration of the monsoon precipitation and a maximum SST center. Note that the maximum SST center is located at approximately a 10° longitude east of the eastward-extended precipitation center. The black line in Figure 1 can be used to estimate the eastward phase speed of these atmospheric and oceanic fields.

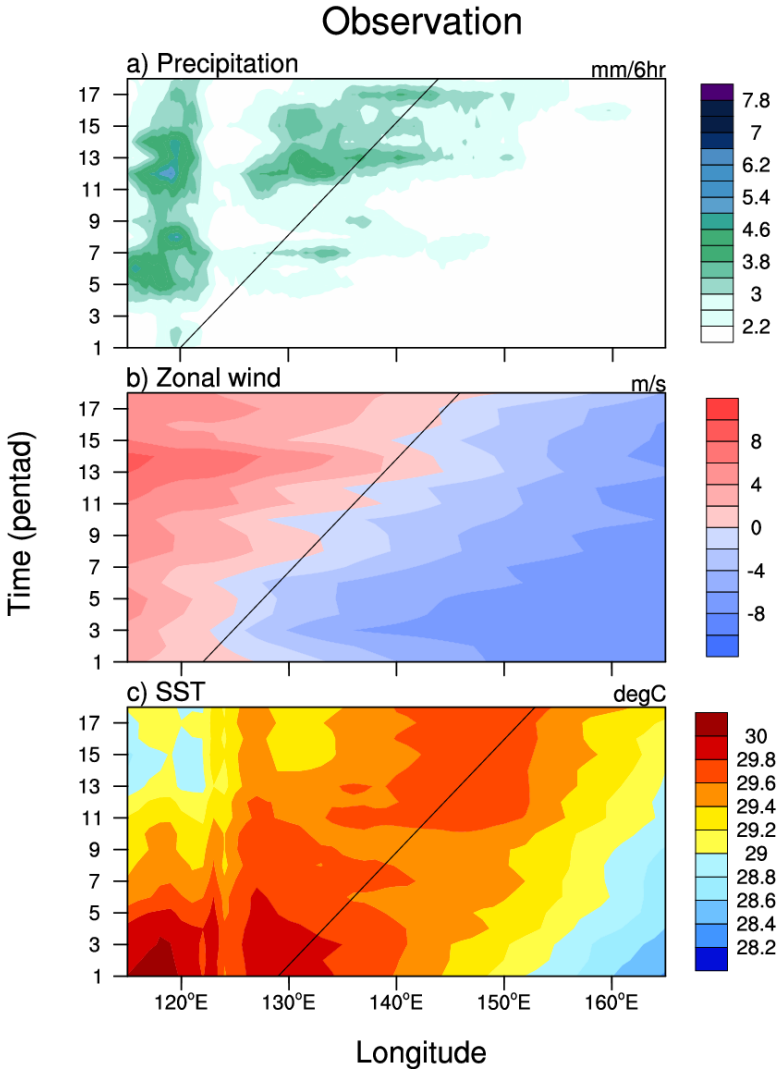

Figure 1. Hovmoller diagrams of climatological pentad mean (**a**) precipitation (unit: mm/6 h), (**b**) zonal wind (unit: ms^{-1}) at 850 hPa, and (**c**) SST (unit: °C), averaged over 10° N–15° N, based on observational data. The Y-axis unit is pentad (every 5 days, from June 1 to August 31). Data are derived from TRMM and ERA-interim for a 20-year period (1998–2017).

Figure 2 illustrates the horizontal evolution (four pentad mean) patterns of the precipitation, wind, and SST fields. The red straps in the left panel of Figure 2 clearly show the time progression of the low-level westerly associated with MT. In Pentad 1–4, the rainfall induced by topographically lifting near the west coast of the Philippines is relative weak due to weaker westerlies (Figure 2a). The local rainfall becomes stronger in Pentad 5–8 due to enhanced westerlies (Figure 2b). As time progresses, a second precipitation center appears to the east of the Philippines, even though topographically generated rainfall still exists to the west of the Philippines (Figure 2c). In Pentad 13–16, the eastward penetrating precipitation center covers a large area of WNP, ranging from 130° E to 150° E. Since the focus of the current study is on the eastward extension of the MT, we use a red circle in

Figure 2 to denote the eastward-extending rainfall center. These rainfall centers will be used as a reference point for the subsequent composite analysis.

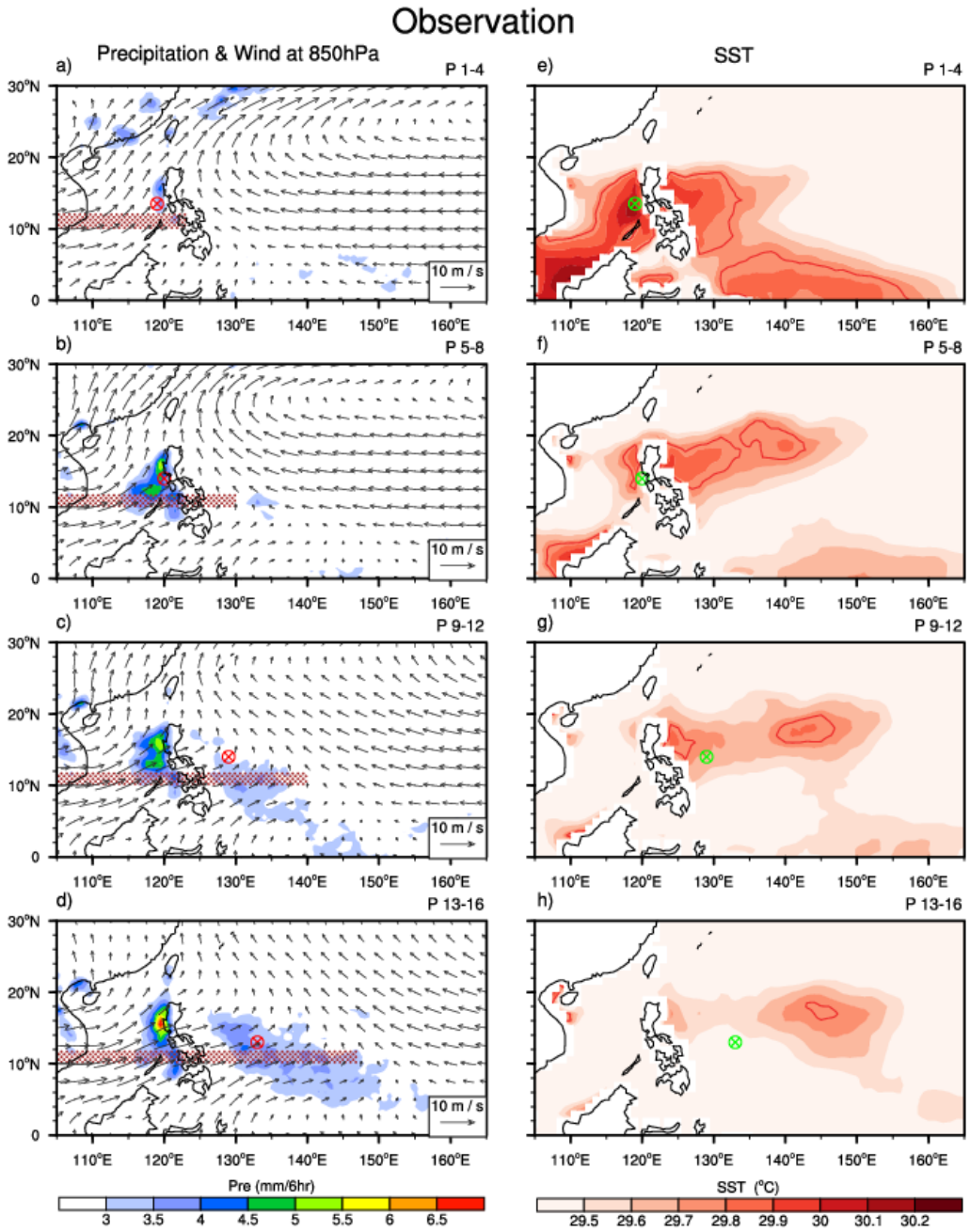

Figure 2. (**a**–**d**) Horizontal evolution (4 pentad mean) patterns of the precipitation (shading; mm/6 h) and wind field (vector; ms^{-1}) at 850 hPa. The red straps show the eastward-extended low-level westerly. (**e**–**h**) Horizontal evolution patterns of SST (shading; °C). The interval is 0.1 °C. The red contour = 29.75 °C. The red and green circles in both the left and right panels denote the eastward-extending MT rainfall centers. Data are derived from ERA-interim and TRMM for a 20-year period (1998–2017).

Accompanied by the eastward extension of the low-level westerly and precipitation is the eastward migration of a maximum SST center, as shown in the right panel of Figure 2). It is clearly seen that along the key MT zone (10° N–20° N) that a maximum SST center tends to appear to the east of the eastward-extended precipitation reference center.

Physically, the occurrence of a maximum SST center to the east of the precipitation center favors the eastward extension of the monsoon convection. According to Lindzen and Nigam [18], a maximum SST center may induce a boundary layer convergence in situ through SST-gradient-induced pressure gradient forces. Ascending motions at the top of the boundary layer associated with the convergence may increase the low-level moisture through vertical moisture advection. The increase in the low-level moisture eventually strengthens the convective instability in situ [19], leading to the eastward extension of the MT.

The argument above implies that the zonally asymmetric precipitation-SST phase relation is a possible mechanism for the eastward extension of the MT. It is worth mentioning that the maximum SST centers are, in general, located to the northeast of the precipitation centers (Figure 2e–h). This implies that the SST tendency is asymmetric relative to the precipitation center. To reveal this feature, we plotted the horizontal maps of the SST tendency and conducted an oceanic mixed layer heat budget diagnosis. Figure 3 shows the horizontal patterns of the composite SST tendency field and associated mixed-layer heat budget terms. The composite is based on the reference precipitation centers from Pentad 1–4 to Pentad 9–12 (Figure 2a–c). Pentad 13–16 is not included in the composite because the eastward extension of the MT at that period had reached the final stage.

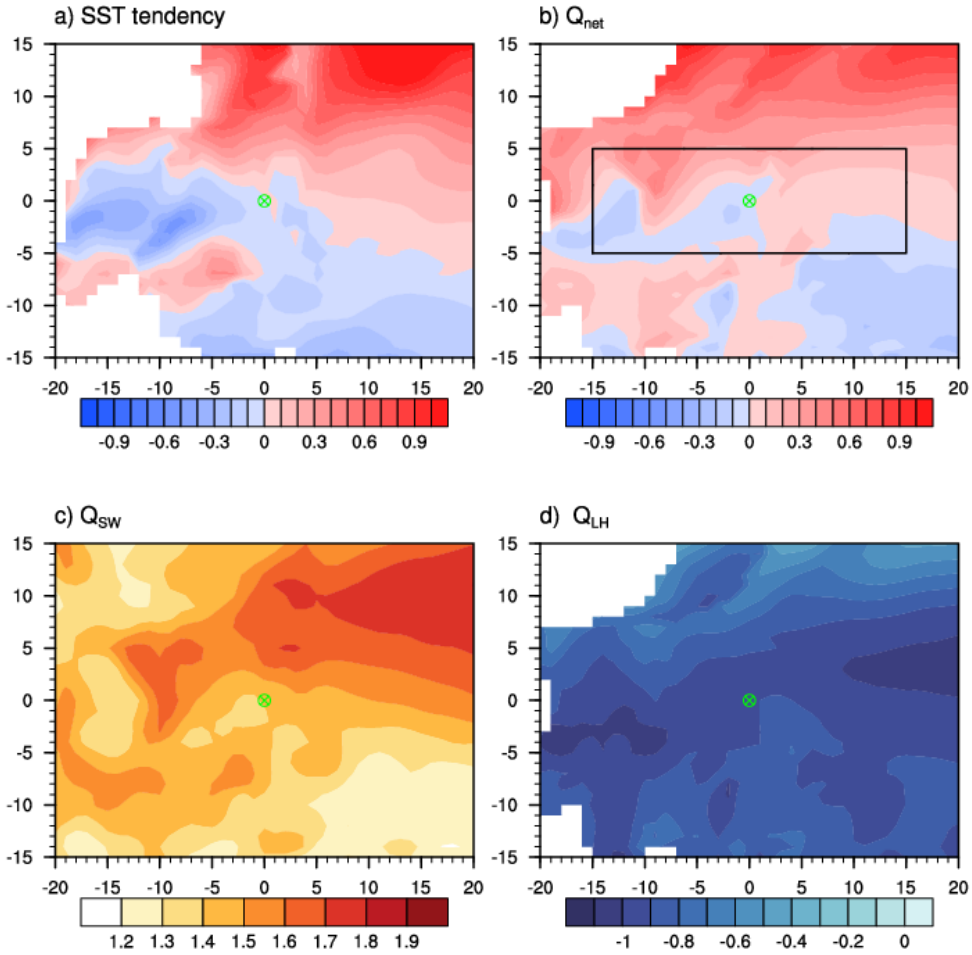

Figure 3. Composite horizontal patterns of (**a**) SST tendency ($\frac{\partial SST}{\partial t}$), (**b**) net surface heat flux term (Q_{net}), (**c**) net surface shortwave radiation (Q_{sw}), and (**d**) net surface latent heat flux (Q_{LH}) based on the reference precipitation centers from Figure 2a–c. All positive values denoting downward. The units of horizontal and vertical axes are degree, and color scale is 0.1 °C 20 day^{-1}. The green circles (0, 0) represent the composite reference rainfall center at (123.7° E, 14° N). The black box area in (**b**) indicates the calculation area for pattern correlation.

The northeastward shift of the SST center relative to the precipitation center is coherent with the asymmetric SST tendency pattern (Figure 3a), which shows a clear northeast-southwest dipole pattern, with positive (negative) values to the northeast (southwest). The composite net heat flux pattern resembles the SST tendency pattern (Figure 3b), which implies that the net surface heat flux field is critical in causing the SST tendency asymmetry. This is not surprising because ocean advective processes are, in general, small in the warm pool region where the mean thermocline is deep, and the mean horizontal temperature gradient is weak. In fact, our calculation shows that the ocean temperature advection fields as well as the surface longwave radiative and sensible heat fluxes are negligibly small (figures not shown). Two dominant terms in the surface heat flux fields are downward shortwave radiation and surface latent heat flux, as shown in Figure 3c,d. It is noted that the pattern of the shortwave radiation field resembles the net surface heat flux field, with a clear northwest-southeast asymmetry (Figure 3c). In fact, the pattern correlation of the two fields is 0.75 in the black box area of Figure 3b. The asymmetric shortwave radiation pattern is mainly attributed to the asymmetry in the cloud pattern: while the increased cloud cover happens in and to the west of the reference precipitation center, it is cloud-free to its east due to the occurrence of the subtropical high. The surface latent heat flux pattern (Figure 3d), on the other hand, differs markedly from the net heat flux field (Figure 3b). A pair of negative latent heat flux centers appear to both the northeast and southwest of the reference center, with no evident northeast-southwest asymmetry. Therefore, the main driver to cause the asymmetric SST tendency pattern arises from the shortwave radiation impact.

In addition to the air–sea interaction process mentioned above, lower-tropospheric moisture advection also contributes to the eastward extension of the MT. Figure 4a shows the composite horizontal patterns of lower-tropospheric wind and moisture advection fields. Again, the composite is based on the precipitation reference centers for Pentad 1–12. Note that large lower-tropospheric moisture advection appears to the southeast of the precipitation reference center (Figure 4a). The orientation of the moisture advection field is in line with lower-tropospheric southeasterlies, which are part of the WNP subtropical high. Physically, enhanced moisture advection would lead to the increase in low-level moisture to the east of the convective center, promoting the eastward extension of the MT.

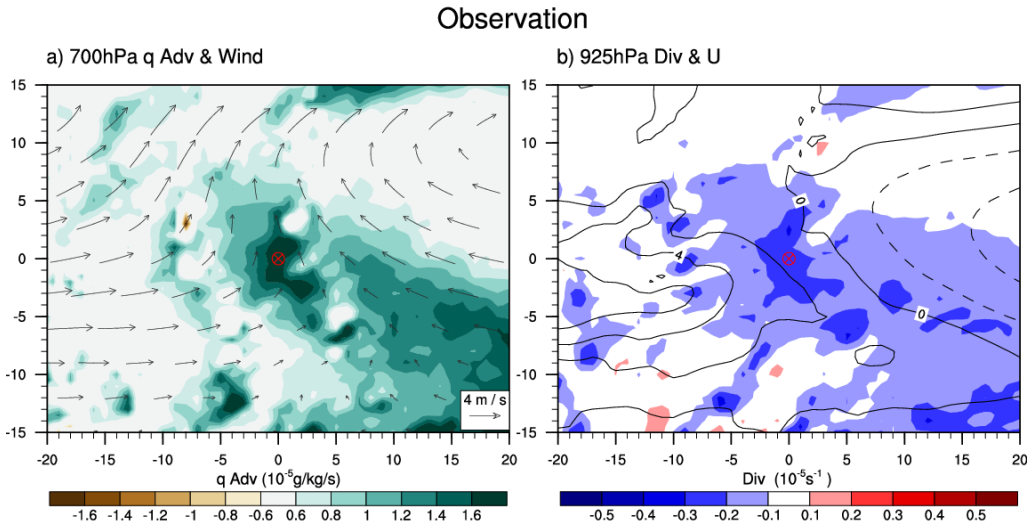

Figure 4. Composite horizontal patterns of (**a**) observed moisture advection (shading; 10^{-5}g/kg/s) and wind field (vector; ms^{-1}) at 700 hPa; (**b**) divergence (shading; 10^{-5}s^{-1}) and zonal wind (contour; ms^{-1}) at 925 hPa. The red circles (0, 0) represent the composite reference rainfall center. The composite is performed based on the eastward propagation stage from Pentad 1–4 to Pentad 9–12.

Another noted feature is the occurrence of boundary layer convergence to the east of the precipitation reference center (Figure 4b). It is likely that the convergence results from the condensational heating induced the Kelvin wave response [19]. Precipitation along

lower latitudes would project an equatorially symmetric component, which, according to Gill [20], would induce a Kelvin wave response, with lower-tropospheric easterly and low-pressure fields appearing to the east of the precipitation center. The so-generated low pressure further induces a boundary-layer convergence in situ [21]. A further diagnosis shows that the boundary layer convergence arises primarily from the zonal wind component, as boundary layer westerlies are located at and to the west of the precipitation center (Figure 4b). The zonal asymmetry of the boundary-layer convergence favors the development of shallow and congestus convection to the east of the precipitation center, leading to the eastward extension of the MT. Therefore, two internal atmospheric mechanisms in addition to the air–sea interaction mechanism are revealed through the current observational analysis. The two internal atmospheric mechanisms, as well as the SST forcing mechanism, will be further tested in the subsequent idealized numerical model experiments.

4. Idealized Numerical Simulations

Two sets of numerical experiments were carried out to reveal the roles of the internal atmospheric processes and the air–sea interaction process in causing the eastward extension of the MT. In the CTL experiment, a realistic time-dependent climatological SST was specified. In the FIX_SST experiment, SST was specified at the climatological June 1 values.

Same as Figure 1, Figure 5 shows the time–longitude sections of the simulated climatological pentad mean fields from both CTL and FIX_SST. As the model simulated MT shifted slightly northward compared to the observed, we examined the simulated precipitation and 850hPa zonal wind fields, along with the specified SST, averaged over 12° N–17° N.

The eastward extension of the simulated zonal wind and precipitation fields well resembled the observed. For example, the monsoon westerlies were located near 130° E in early June and gradually extended eastward and reached to the east of 150° E in late August. Perhaps the most striking feature of Figure 5 is that the monsoon trough could still penetrate eastward, even in the absence of the time-dependent SST forcing. This FIX_SST experiment alone confirmed the role of internal atmospheric processes. On the other hand, there was a clear difference in the extent of the eastward extension between the CTL and FIX_SST. In CTL (left panel), the westerly and precipitation fields extended continuously eastward during the entire summer period, in a way similar to the observed. This is in contrast to FIX_SST, in which the zonal extent of the low-level westerly was confined to the west of 145° E.

The horizontal evolution patterns of the simulated precipitation and 850 hPa wind fields in the CTL (left panel) and FIX_SST (right panel) are shown in Figure 6. Compared to the observation, there is a systematic bias in the simulated rainfall field east of the Philippines in CTL. Despite the bias, the model is able to simulate the eastward extension of the precipitation and low-level westerly fields. The warmest SST center appears to the east of the precipitation center, in a way similar to the observed. In FIX_SST, the eastward extension of the low-level westerly and precipitation fields is weaker and less evident, compared to CTL. In addition to the eastward-extension difference, the FIX_SST simulates a stronger topographically induced precipitation center near the west coast of the Philippines.

To reveal specific atmospheric processes that give rise to the eastward extension of the MT in FIX_SST, we made a similar composite analysis as in Figure 4. Figure 7a shows the horizontal patterns of the composite lower-tropospheric moisture advection and wind fields at 700 hPa. In the absence of the time-dependent SST forcing, an asymmetric lower-tropospheric moisture advection pattern occurs. A large moisture advection appears to the southeast of the precipitation reference center, and the wet advective belt is in line with the lower-tropospheric wind vector. As in the observation, the large moisture advection arises from both horizontal and vertical advection components.

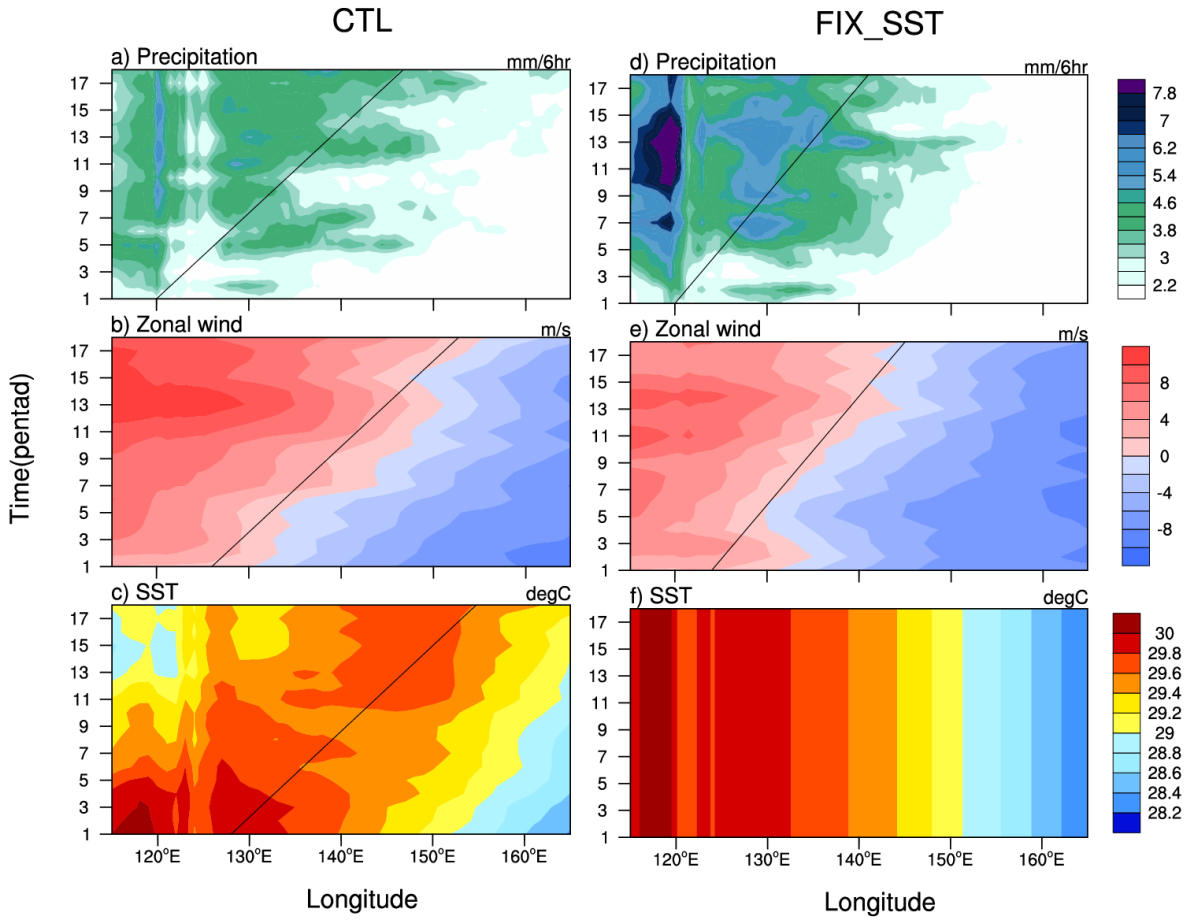

Figure 5. Hovmoller diagrams of climatological pentad-mean (**a**) precipitation (unit: mm/6 h), (**b**) zonal wind (unit: ms^{-1}) at 850 hPa, and (**c**) SST (unit: °C) for the control experiments (CTL, left panel). (**d**–**f**) (right panel): Same as in (**a**–**c**) except for the Sensitivity experiments (FIX_SST). The averaged latitude strip for both CTL and FIX_SST is from 12° N to 17° N.

Figure 7b illustrates the composite pattern of the simulated zonal wind and divergence fields at 925 hPa in FIX_SST. There is a clear asymmetry in the boundary layer divergence field relative to the precipitation reference center. A large-scale boundary convergence appears at and to the east of the convective center. The eastward shift of the boundary layer convergence arises primarily from the zonal wind contribution, as the boundary layer westerly shifts eastward and is, approximately, in phase with the precipitation center [21]. As discussed in the previous section, the asymmetric convergence field is likely a consequence of the Kelvin wave response to the convective heating [19].

Therefore, the FIX_SST experiment confirms the roles of asymmetric lower-tropospheric moisture advection and boundary-layer convergence in promoting the eastward expansion of the MT. Together with the CTL experiment, the idealized numerical experiments confirm the observational analysis result that both the internal atmospheric processes and the air–sea interaction processes contribute to the eastward extension of the MT.

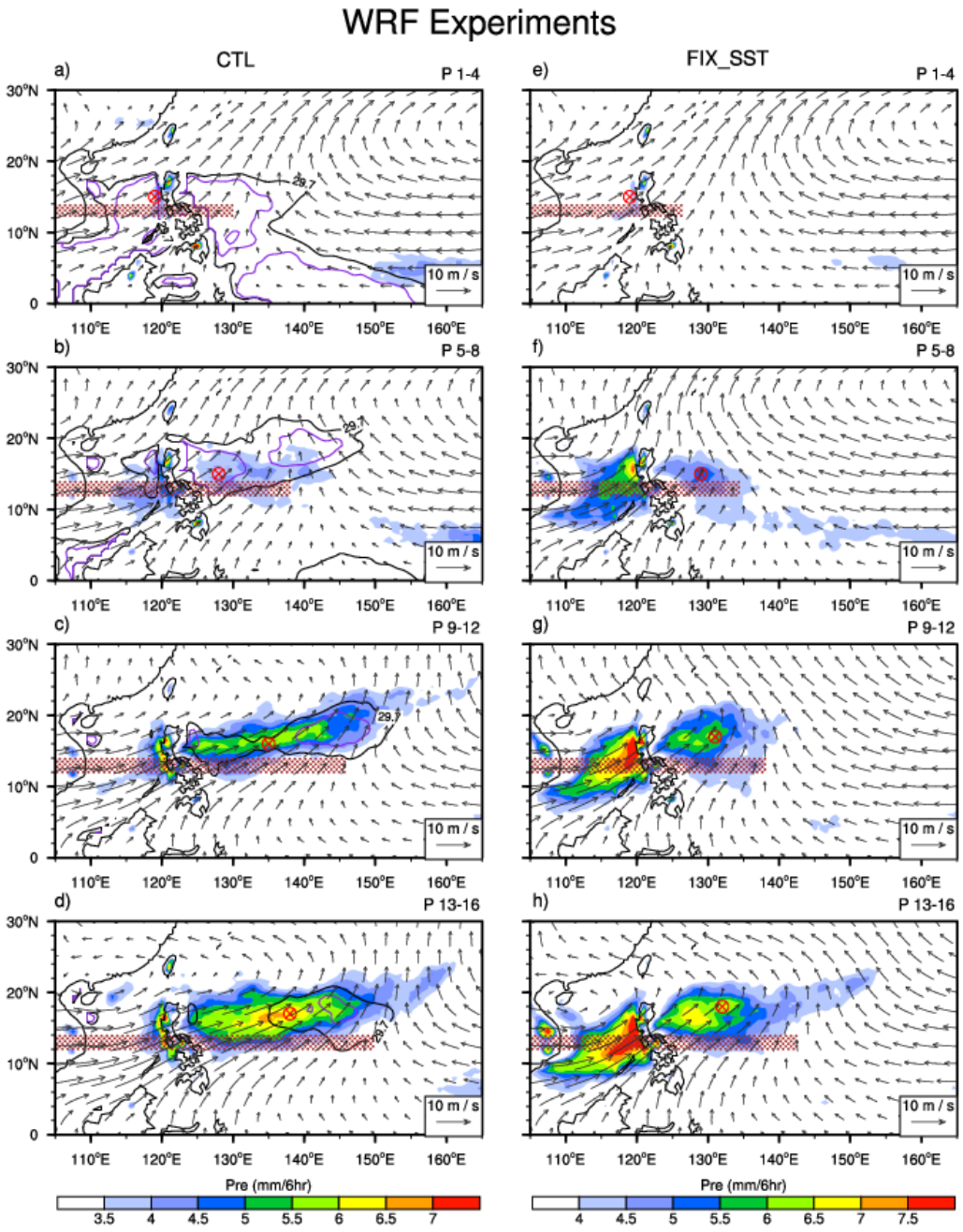

Figure 6. (**a**–**d**) Horizontal evolution (4 pentad mean) patterns of the precipitation (shading; mm/6 h) and 850 hPa wind (vector; ms^{-1}) fields in CTL (left panel). (**e**–**h**) (right panel): Same as in (**a**–**d**) except in FIX_SST. Contours in the left panel represent SST (unit: °C), with the purple contour denoting 29.8 °C. The red straps show the eastward-extended low-level westerly. Red circles denote eastward-expanding MT rainfall centers.

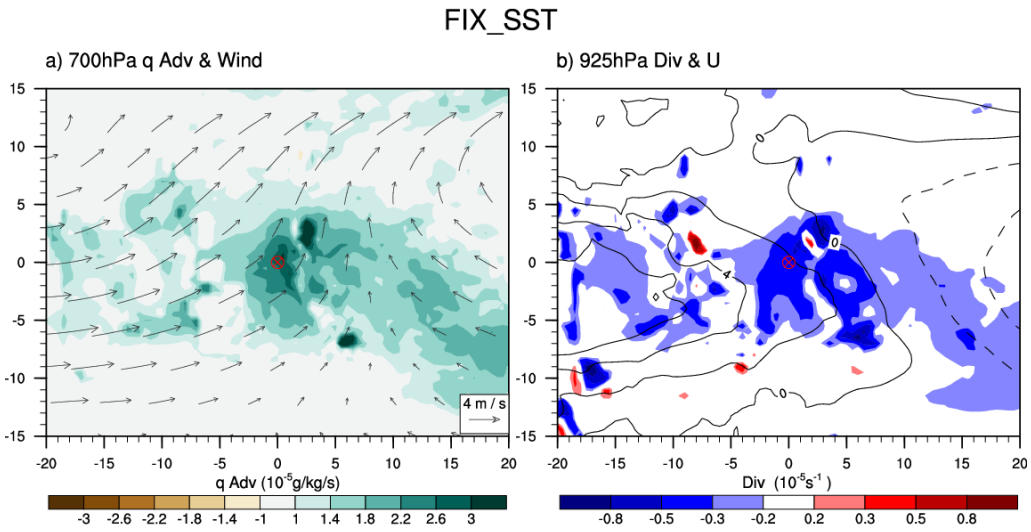

Figure 7. Composite horizontal patterns of (**a**) lower-tropospheric (700 hPa) moisture advection (shading; 10^{-5}g/kg/s) and wind (vector; ms^{-1}) fields and (**b**) boundary-layer (925 hPa) divergence (shading; 10^{-5}s^{-1}) and zonal wind (contour; ms^{-1}) fields in the FIX_SST experiments. The red circles represent the composite reference rainfall centers.

5. Conclusions and Discussion

In this study, we investigated the mechanisms responsible for the eastward extension of the climatological monsoon trough (MT) over the western North Pacific (WNP) in the boreal summer. We took both observational analysis and numerical modeling approaches.

Our observational analyses showed that the eastward extension of the monsoon westerlies and precipitation from June to August were attributed to both the air–sea interaction and the atmospheric internal dynamics. It was noted that a warm SST center was located to the east of the precipitation center. This asymmetric SST distribution may have induces a boundary layer convergence east of the convection through SST-gradient induced pressure gradient forces [18]. The asymmetric boundary layer convergence and associated vertical motion (via vertical moisture advection) promoted convectively unstable stratification in situ, leading to the eastward extension of the MT. A mixed layer heat budget diagnosis indicated that the asymmetric SST tendency pattern arose primarily from the asymmetry of the downward shortwave radiation, while other heat flux terms and ocean advections play a minor role. The asymmetry of the downward shortwave radiative flux was attributed to cloud asymmetry. While there was clear sky to the northeast of the precipitation center, a large cloud cover appeared at and to the southwest of the precipitation center.

In addition to the air–sea interaction process, asymmetric lower-tropospheric moisture advection also played a role. Southeasterlies to the west of the subtropical high advect high mean moisture from the south, leading to a positive moisture tendency, which helps setup a convectively unstable stratification to the east of the convection. Meanwhile, the heating-induced Kelvin wave zonal wind response also promoted a boundary layer convergence to the east, which favored the development of a new convection to the east.

To confirm the proposed internal atmospheric mechanisms, we conducted idealized numerical model experiments. Two sets of WRF experiments were carried out. In the control experiment, the model was forced by a realistic time-dependent SST field. In the sensitivity experiment, the SST was fixed at its June 1st climatological values. While the control experiment successfully simulated the eastward extension of the MT, the sensitivity experiment also captured the eastward extension, but to a lesser extent. A diagnosis of the sensitivity experiment indicated the roles of two internal atmospheric processes. One was the asymmetric lower-tropospheric moisture advection and the other was asymmetric boundary layer divergence. Thus, the combined numerical experiments pointed out

the importance of both the air–sea interaction and the internal atmospheric processes in promoting the sub-seasonal eastward progression of the MT.

In this study, we focused on the sub-seasonal evolution of the climatological MT in the boreal summer over WNP. Previous studies found that the WNP MT varied over multiple timescales, ranging from synoptic to interannual and interdecadal timescales [1,22,23]. Various atmospheric and coupled atmosphere–ocean models have been used to predict the WNP monsoon variabilities [24,25]. Given that the multi-scale variabilities evolve under the unique WNP climate mean state, it is conceivable that good predictive skill relies on the successful simulation of the temporally evolving climatological mean state. It is anticipated that the advance of the current understanding of the sub-seasonal evolution of the monsoon trough would help to diagnose the model errors and improve the representation of model physics, so that the prediction skill of the MT and its variability can be increased.

While the current study emphasizes the importance of air–sea interaction and internal atmospheric dynamics, it is worth mentioning that ocean dynamics may also play a role. The east of Indonesia is subject to the reflection of the Rossby waves in response to the tropical wind stress forcing [26]. These waves may induce a significant change in the ocean thermocline in WNP, resulting in the eastward extension of the warm pool and precipitation. This possibility will be explored in future endeavors.

Author Contributions: Conceptualization, C.Q. and T.L.; methodology, C.Q.; software, C.Q.; formal analysis, C.Q.; writing—original draft preparation, C.Q.; writing—review and editing, T.L.; visualization, C.Q.; funding acquisition, T.L. All authors have read and agreed to the published version of the manuscript.

Funding: This research was funded by National Natural Science Foundation of China (NSFC), grant number 42088101.

Institutional Review Board Statement: Not applicable.

Informed Consent Statement: Not applicable.

Data Availability Statement: European Centre for Medium-range Weather Forecast (ECMWF) (2011): The ERA-Interim reanalysis dataset, Copernicus Climate Change Service (C3S), available from https://www.ecmwf.int/en/forecasts/datasets/archive-datasets/reanalysis-datasets/era-interim (accessed on 13 March 2023).

Acknowledgments: This study was supported by NSFC Grant 42088101. The authors acknowledge the High-Performance Computing Center of Nanjing University of Information Science and Technology for their support of this work.

Conflicts of Interest: The authors declare no conflict of interest.

References

1. Li, T.; Wang, B. A review on the western North Pacific monsoon: Synoptic-to-interannual variabilities. *Terr. Atmos. Ocean Sci.* **2005**, *16*, 285–314. [CrossRef] [PubMed]
2. Li, T.; Hsu, P.C. *Fundamentals of Tropical Climate Dynamics*; Chapter 4: Tropical Cyclone Formation; Text Book; Springer Atmospheric Sciences: Cham, Switzerland, 2017; ISBN 978-3-319-59595-4. [CrossRef]
3. Gray, W.M. Global View of the Origin of Tropical Disturbances and Storms. *Mon. Weather Rev.* **1968**, *96*, 669–700. [CrossRef]
4. Harr, P.A.; Chan, J.C.L. *Monsoon Impacts on Tropical Cyclone Variability*; WMO Tech. Doc. 1266, TMPR Rep. 70; WMO: Geneva, Switzerland, 2005; pp. 512–542.
5. Li, T. *Synoptic and Climate Aspects of Tropical Cyclogenesis in Western North Pacific*; Oouchi, K., Fudeyasu, H., Eds.; Nova Science Publishers, Inc.: Hauppauge, NY, USA, 2012; Chapter 3; pp. 61–94.
6. Li, T.; Ge, X.; Wang, B.; Zhu, Y. Tropical Cyclogenesis Associated with Rossby Wave Energy Dispersion of a Preexisting Typhoon. Part II: Numerical Simulations. *J. Atmos. Sci.* **2006**, *63*, 1390–1409. [CrossRef]
7. Zong, H.; Wu, L. Re-examination of tropical cyclone formation in monsoon troughs over the western North Pacific. *Adv. Atmos. Sci.* **2015**, *32*, 924–934. [CrossRef]
8. Wang, B.; Clemens, S.C.; Ping, L. Contrasting the Indian and East Asian monsoons: Implications on geologic timescales. *Mar. Geol.* **2003**, *201*, 5–21. [CrossRef]
9. Qin, C.; Li, T.; Liu, J.; Bi, M. A Mechanism for Formation of the Western North Pacific Monsoon Trough: Nonlinear Upscale Cascade. *Clim. Dyn.* **2021**, *56*, 3889–3898. [CrossRef]

10. Kuo, H.C.; Chen, J.H.; Williams, R.T.; Chang, C.P. Rossby Waves in Zonally Opposing Mean Flow: Behavior in Northwest Pacific Summer Monsoon. *J. Atmos. Sci.* **2001**, *58*, 1035–1050. [CrossRef]
11. Fu, B.; Li, T.; Peng, M.S.; Weng, F. Analysis of Tropical Cyclogenesis in the Western North Pacific for 2000 and 2001. *Weather Forecast.* **2006**, *22*, 763–780. [CrossRef]
12. Wu, R.; Wang, B. Multi-stage Onset of the Summer Monsoon over the western North Pacific. *Clim. Dyn.* **2001**, *17*, 277–289. [CrossRef]
13. Wu, R. Processes for the northeastward advance of the summer monsoon over the western North Pacific. *J. Meteorol. Soc. Jpn. Ser. II* **2002**, *80*, 67–83. [CrossRef]
14. Uppala, S.M.; Dee, D.; Kobayashi, S.; Berrisford, P.; Simmons, A. Towards a Climate Data Assimilation System: Status Update of ERA-Interim. 2008. Available online: https://www.ecmwf.int/publications/newsletters/pdf/115_rev.pdf (accessed on 1 January 2008).
15. Huffman, G.J.; Adler, R.F.; Bolvin, D.T.; Gu, G.; Nelkin, E.J.; Bowman, K.P.; Hong, Y.; Stocker, E.F.; Wolff, D.B. The TRMM Multisatellite Precipitation Analysis (TMPA): Quasi-Global, Multiyear, Combined-Sensor Precipitation Estimates at Fine Scales. *J. Hydrometeorol.* **2007**, *8*, 38–55. [CrossRef]
16. Cao, X.; Li, T.; Peng, M.; Chen, W.; Chen, G. Effects of Monsoon trough Intraseasonal Oscillation on Tropical Cyclogenesis over the Western North Pacific. *J. Atmos. Sci.* **2014**, *71*, 4639–4660. [CrossRef]
17. Li, T. Relative Role of Dynamic and Thermodynamic Processes in the Development of the Indian Ocean Dipole: An OGCM diagnosis. *Geophys. Res. Lett.* **2002**, *29*, 25-1–25-4. [CrossRef]
18. Lindzen, R.S.; Nigam, S. On the Role of Sea Surface Temperature Gradients in Forcing Low-Level Winds and Convergence in the Tropics. *J. Atmos.* **1987**, *45*, 2418–2436. [CrossRef]
19. Hsu, P.C.; Li, T. Is "rich-get-richer" valid for Indian Ocean and Atlantic ITCZ? *Geophys. Res. Lett.* **2012**, *39*, L13705. [CrossRef]
20. Gill, A.E. Some Simple Solutions for Heat-Induced Tropical Circulation. *Quart. J. Roy. Meteor. Soc.* **1980**, *106*, 447–462. [CrossRef]
21. Wang, B.; Li, T. A Simple Tropical Atmosphere Model of Relevance to Short-Term Climate Variations. *J. Atmos. Sci.* **1993**, *50*, 260–284. [CrossRef]
22. Harr, P.A.; Chun-Chieh, W. Tropical Cyclone Characteristics and Monsoon CIrculations. In *The Global Monsoon System: Research and Forecast*; Chang, C.P., Ding, Y., Lau, N.C., Johnson, R.H., Wang, B., Yasunari, T., Eds.; World Scientific Publishing: Singapore, 2011; pp. 357–372.
23. Wu, L.; Wen, Z.; Huang, R.; Wu, R. Possible Linkage between the Monsoon Trough Variability and the Tropical Cyclone Activity over the Western North Pacific. *Mon. Weather Rev.* **2012**, *140*, 140–150. [CrossRef]
24. Li, C.; Lu, R.; Chen, G. Promising Prediction of the MonsoonTrough and Its Implication for Tropical Cyclone Activity over the Western North Pacific. *Environ. Res. Lett.* **2017**, *12*, 074027. [CrossRef]
25. Wang, C.; Wu, L. Future Changes of the Monsoon Trough: Sensitivity to Sea Surface Temperature Gradient and Implications for Tropical Cyclone Activity. *Earth's Future* **2018**, *6*, 919–936. [CrossRef]
26. Pinault, J.-L. Long Wave Resonance in Tropical Oceans and Implications on Climate: The Pacific Ocean. *Pure Appl. Geophys.* **2015**, *173*, 2119–2145. [CrossRef]